Catalysis Science & Technology

Accepted Manuscript

This is an *Accepted Manuscript*, which has been through the Royal Society of Chemistry peer review process and has been accepted for publication.

Accepted Manuscripts are published online shortly after acceptance, before technical editing, formatting and proof reading. Using this free service, authors can make their results available to the community, in citable form, before we publish the edited article. We will replace this *Accepted Manuscript* with the edited and formatted *Advance Article* as soon as it is available.

You can find more information about *Accepted Manuscripts* in the Information for Authors.

Please note that technical editing may introduce minor changes to the text and/or graphics, which may alter content. The journal's standard Terms & Conditions and the Ethical guidelines still apply. In no event shall the Royal Society of Chemistry be held responsible for any errors or omissions in this *Accepted Manuscript* or any consequences arising from the use of any information it contains.

ROYAL SOCIETY OF CHEMISTRY

www.rsc.org/catalysis

An *Ab Initio* Thermodynamics Study of Cobalt Surface Phases under Ethanol Steam Reforming Conditions

Wenjia Luo and Aravind Asthagiri*

William G. Lowrie Department of Chemical and Biomolecular Engineering,
The Ohio State University, Columbus, OH, 43210, USA

*To whom correspondence should be addressed, asthagiri.1@osu.edu

Tel: 614-688-8882, Fax: 614-292-3769

Catalysis Science & Technology Accepted Manuscript

Abstract

Co based materials have emerged as promising ethanol steam reforming (ESR) catalysts in recent years. Both Co^0 (Co metal) and Co^{2+} (CoO oxide) states were found to exist in the catalyst under reaction conditions and contribute to the catalytic activity, although their separate roles are still not fully understood. Density function theory (DFT) calculations were carried out to explore possible surface configurations based on the (100) and (111) facets of CoO. *Ab initio* atomistic thermodynamics was then applied to study the relative stability of various surface structures of Co^0/Co^{2+} under ESR reaction conditions where H_2O and H_2 are the most abundant component in the gas phase. Based on the surface phase diagrams of CoO(100), CoO(111), and general Co^0/Co^{2+} catalyst, we found that the clean CoO(100) and OH* covered CoO(111) are the most Co^{2+} surface configurations under ESR reaction conditions. We also suggest that a reducible support may be important in stabilizing the Co^{2+} surfaces against reduction into metallic Co surfaces. The stable surface configurations of CoO identified in this paper can guide future DFT studies on the ESR catalytic activity of Co^{2+}.

Catalysis Science & Technology Accepted Manuscript

1. Introduction

Hydrogen in fuel cells is a promising energy source for the future because of its high efficiency and environmental friendliness [1]. Ethanol steam reforming (ESR) [$C_2H_5OH + 3H_2O \rightarrow 2CO_2 + 6\ H_2$] provides a renewable route of hydrogen production since ethanol can be obtained from fermentation of biomass[2]. On site or on demand steam reforming can also overcome the difficulty in hydrogen storage and distribution. In recent years, much attention has been focused on the development of ESR catalysts with high activity, stability, and selectivity to CO_2 [3].

While noble metal based materials, including Ru, Pt, and especially Rh, have shown fast reaction rate and high selectivity towards CO_2[4, 5], the high cost of these materials is a drawback. Recently, less expensive Co-based materials have emerged as efficient ESR catalysts [6-12]. With improvements in the support materials and preparation procedures, Co-based catalysts, such as Co supported on ceria, can achieve high H_2 yield (> 90%) at fast space velocities (~ 10000 h^{-1}) [12-14]. This excellent performance of ceria supported Co has been attributed to the ability of Co to break the C-C bond at relatively low temperatures (523 – 673 K) and the high oxygen mobility of the ceria support[7, 8, 15-17]. Despite these advantages, by-products such as CO, CH_4 and C_2H_4 are still present on Co-based catalysts under ESR conditions, which limit the hydrogen conversion rate[12]. Furthermore, Co-based catalysts still lack long term stability due to the carbon deposition and Co sintering problems[11].

Further improvement of Co-based ESR catalysts requires a fundamental understanding of the reaction mechanisms on the catalyst surfaces. An important but

Catalysis Science & Technology Accepted Manuscript

unresolved question is the exact nature of the active site on Co-based ESR catalysts. It has been reported in various studies that two oxidation states of Co, namely Co^0 and Co^{2+}, reach an equilibrium state under ESR reaction conditions [8, 15, 18-22]. It is also interesting to note that Co_3O_4 has no ESR catalytic activity unless it is reduced to a mixture of Co^0 and Co^{2+}. [19, 22, 23]

Presence of both Co^0 and Co^{2+} under ESR reaction conditions leads to questions about their separate contributions to the catalytic activity. Some researchers have proposed that Co^0 is the only important site in ESR reactions since it provides activity for C-C bond breaking and ethanol conversion [24, 25]. They suggest that preventing Co^0 from being oxidized into Co^{2+} is the key to achieve high ESR activity. On the other hand, other researchers have indicated that keeping a proper Co^{2+}/Co^0 ratio was crucial to maintain the activity and stability of the catalysts[26, 27]. Recently, Martono and co-workers provided new insights for the specific roles of Co^{2+} through ultrahigh vacuum (UHV) studies of Co supported on oxide surfaces [28-30]. They showed that the Co^0 sites catalyzed the decarbonylation of ethanol into methyl, further decomposition of which caused carbon deposition, while the Co^{2+} sites facilitates ethanol dehydrogenation into acetaldehyde. However their experiments did not provide information about the further conversion of acetaldehyde. Song et al. also showed that the high mobility of oxygen is crucial for achieving high CO_2 selectivity and in the same time preventing coking and sintering of the Co catalysts[16, 17], but how Co^{2+} sites are involved in the catalytic reactions is still not clear.

Coexistence of Co^0 and Co^{2+} was observed on a wide range of supports such as ceria, titania, and zinc oxide[9, 17, 18]. Co^{2+} can either exist in a separate CoO phase, or form

Catalysis Science & Technology Accepted Manuscript

mixed oxides with metal atoms in the support. Recent experiments showed that CoO[200] and CoO[111] planes can be observed by *in situ* X-ray diffractometry (XRD) under ESR reaction conditions[22]. Furthermore, studies where $CoAl_2O_4$ mixed oxides and CoO-MgO solid solutions formed in Co/Al_2O_3 and Co/MgO catalysts were not active towards ESR reactions[25, 27]. Based on these results, in this study we focus on CoO as a representation of Co^{2+} and study the stability of its surface structures. Observations made in this paper can promote the understanding of the catalytic activities of Co^{2+} and Co^0 components in ESR reactions. Although in the real catalytic system the interface between Co and the oxide support may influence both the stability of the Co oxide phase and serve as active sites, the current study can serve as a prerequisite before such complex effects are fully explored.

First-principles methods such as density functional theory (DFT) and *ab initio* atomistic thermodynamics have been used to study the catalytic activity of Co catalysts[31-33]. Ma and co-workers have examined possible ESR pathways on the metallic Co(0001) surface[31]. Wang et al. have studied ethanol decomposition mechanisms on all group VIII metal surfaces including Co(111)[32]. Since Co_3O_4 is a well-known catalyst for CO oxidation, there are also numerous DFT studies on the catalytic activity of Co_3O_4[33-35]. However as far as we know, there is no first-principles study on the catalytic activity of CoO in ESR reactions. Absence of studies on this topic may be partly due to the complex nature of metal oxide surfaces and their strong dependence on environmental conditions. For example, a recent study showed that surface structures of $CeO_2(111)$ were sensitive to the temperature and the partial pressures of H_2O and O_2[36]. Under ESR conditions the CoO surfaces are exposed to a mixture of steam, hydrogen, ethanol, carbon monoxide,

Catalysis Science & Technology Accepted Manuscript

carbon dioxide, and many other ESR intermediates and by-products. No theoretical study has modeled the surface structures of CoO under ESR conditions before, and there are only preliminary experimental and theoretical studies on CoO surfaces under UHV conditions or in the presence of O_2 and H_2O[37-39].

In this paper, we model the surface structures of CoO with the goal to determine the most stable structures of Co catalysts under ESR reaction conditions. We examined two facets of CoO, namely CoO(100) and CoO(111). To simplify the problem, we assumed that the CoO surfaces were in equilibrium with an atmosphere consisted of H_2O and H_2, which are the most abundant gas phase components under ESR reaction conditions. By employing DFT + U[40, 41] and *ab initio* atomistic thermodynamics methods[42-44], we were able to determine the relative stability of different CoO surface configurations under varying temperatures and partial pressures of H_2O and H_2. Since under ESR conditions both Co^0 and Co^{2+} exist, we also calculated the surface free energies of various metallic Co(0001) configurations, and compared the relative stability between Co^0 and Co^{2+} surfaces. We predict Co metal surfaces are more stable than CoO surfaces, which suggests that a reducible support may be very important in stabilizing the Co^{2+} phase under ESR conditions. While we do not explore ESR reaction pathways catalyzed by Co^{2+} sites, the results presented in this paper provide specific CoO surface structures to focus future DFT studies exploring the catalytic role of CoO.

Catalysis Science & Technology Accepted Manuscript

2. Methods

2.1 DFT-GGA + U calculations

We have modeled both the CoO(100) and CoO(111) surfaces with the rocksalt structure. Symmetric supercells were built and adsorbates were placed on both sides (with central inversion symmetry) to study the stability of different surface configurations. The CoO(100) was modeled by a 2 × 2 unit cell containing 5 atomic layers with 8 atoms on each layer. The outer 2 layers on both sides were allowed to move during structural relaxation while the central layer was fixed in its bulk position, although we observed very small displacements (< 0.05 Å) of atoms in the sub-surface layer during structural relaxation. The Co-terminated (Co-term) CoO(111) was also modeled by a 2 × 2 unit cell containing 7 atomic layers with 4 atoms on each layer. The central 3 layers were fixed in their bulk structure. The supercells for CoO(100) and Co-term CoO(111) used in our calculations were illustrated in Fig. 1. The O-terminated (O-term) CoO(111) was similar to Co-term CoO(111) except that an extra layer of O atoms were placed on top of both sides. Experimental lattice constant of 4.261 Å[45] was used for all CoO structures and the reason is explained later in this section. All structures contained a vacuum space of 15 Å between adjacent slabs and were modeled with 3×3×1 Monkhorst-Pack k-point mesh[46]. In this study we also studied the metallic Co(0001) surface configurations, which were modeled by a 2 × 2 unit cell containing 5 atomic layers with 4 atoms on each layer. Experimental lattice constants of a = 2.497 and a/c = 1.633 were used for Co(0001)[47]. The k-point mesh used for the Co(0001) slabs was also 3×3×1.

Catalysis Science & Technology Accepted Manuscript

Spin-polarization was included in all calculations. Metallic Co was set to ferromagnetic in all calculations. CoO exhibits type-II antiferromagnetism (AFM-II) below its Néel temperature of 291 K[48]. In this type of magnetic configuration, spins of Co ions are altering along a <111> direction, while within each (111) plane perpendicular to this aforementioned direction, the spins are parallel to each other. A visualized presentation of this magnetic configuration was provided by Deng et al.[49] In our calculations we also confirmed that AFM-II generated lower electronic energy than any other magnetic configurations for both the bulk and the surface structures. In order to get a consistent result we always set the magnetic configurations in our slab structures to AFM-II. It should also be noted that in CoO(111) the direction of spin alteration was set to be along $(11\bar{1})$, as illustrated in Fig. 1. This magnetic configuration gave a lower energy than setting the spin alteration direction to be (111), which is parallel to the normal direction of the surface. Therefore in our CoO(100) and CoO(111) structures there are 2 Co ions with up-spin and 2 with down-spin per layer within each unit cell. We are aware that the operating temperature of ESR (573-873K)[50] is well above the Néel temperature of CoO, and CoO should be paramagnetic under ESR conditions[18, 51]. In order to address the possible error caused by paramagnetism, we have tested other magnetic configurations and this is discussed in the Supporting Information (Section S3).

A Hubbard-U correction was included in all DFT calculations (DFT+U method) to address the on-site Coulomb interactions[40, 52]. This was done by adopting the Dudarev approach[53]. Recent studies suggested that the U_{eff} (U_{eff} = U - J) value should be chosen by fitting the reaction energies between different oxide forms relevant for the catalytic reaction [54, 55]. For Co, García-Mota and co-workers showed that a U_{eff} value of 3.5 eV

Catalysis Science & Technology Accepted Manuscript

incorporated in DFT can satisfactorily reproduce the oxidation energy of CoO into Co_3O_4[35]. An earlier work by Wang et al. also showed that a similar U_{eff} value of 3.3 eV can closely predict the band gap of CoO. Based on these results, we used a U_{eff} value of 3.5 eV throughout this study. Choice of the U_{eff} value also affects the optimal lattice constant determined by DFT, as we observed that the lattice constant of rocksalt CoO increased from 4.20 Å to 4.25 Å when different U_{eff} values between 0 eV and 3.5 eV were used (for U_{eff} = 3.5 eV the lattice constant is 4.246 Å), which is similar to the behavior observed by Wdowik et al.[51]. We used the experimentally determined value of 4.261 Å[45] for calculations on all CoO structures in this study. Calculations of the CoO bulk oxidation energy and select surface reaction energies show this choice of lattice constant will not effect the conclusions in this paper.

The DFT + U calculations were performed using the Vienna *ab initio* Simulation Package (VASP)[56-58] with projected augmented wave (PAW) pseudopotentials provided in the VASP database[57, 59]. The generalized gradient approximation (GGA) of Perdew-Burke-Ernzerhof (PBE)[60] was used to describe the exchange-correlation effects. An energy cutoff of 400eV was used in the plane-wave expansion. The self-consistent total-energy iterations were accelerated using Gaussian smearing with width of 0.1 eV. Atom positions were relaxed using a limited memory Broyden-Fletcher-Goldfarb-Shanno (LBFGS) method[61] until forces on all unfixed atoms are less than 0.03 eV/Å.

2.2 *Ab initio* atomistic thermodynamics

Under ESR reaction conditions, stability of CoO surface structures are influenced by the environment, including the temperature and the partial pressures of various gas

Catalysis Science & Technology Accepted Manuscript

components in the surrounding atmosphere. *Ab initio* atomistic thermodynamics can solve problems in this category by assuming the surfaces under study to be in thermodynamic equilibrium with the environment[42-44, 62]. In the case of ESR, multiple components are present in the gas phase including steam, hydrogen, ethanol, carbon monoxide, carbon dioxide, and many other ESR by-products. Although in theory *ab initio* atomistic thermodynamics can be applied to cases where multiple gas components are present, inclusion of more than 2 components makes this model very complicated. Instead we considered two gas components that are most abundant under ESR reaction conditions, namely H_2O and H_2. CoO surfaces were assumed to be in equilibrium with a H_2O and H_2 gas phase reservoir at the same time. The interaction between the CoO surface and other species such as ethanol, acetaldehyde, and carbon monoxide, can be examined through subsequent studies based on the stable surface structure identified by *ab initio* thermodynamics.

Stability of a surface structure is measured by its surface free energy:

$$\gamma(T,\{p_i\}) = \frac{1}{2A}[G^{slab} - \sum_i N_i\mu_i\,(T,p_i)] \qquad (1)$$

Here, G^{slab} is the Gibbs free energy of the slab structure. The subscript i in eqn. (1) refers to the Co, O and H species. The result is normalized by 2 times the surface area, A, since two identical surfaces (top and bottom of the slab) are present in the system. The chemical potential of H was only determined by H_2 in the gas phase reservoir through

$$\mu_H = \frac{1}{2}\mu_{H_2(g)} \qquad (2)$$

However, the chemical potential of O was determined by both H_2O and H_2 through

$$\mu_O = \mu_{H_2O(g)} - \mu_{H_2(g)} \qquad (3)$$

Catalysis Science & Technology Accepted Manuscript

An intuitive way to interpret the above relation is to consider a system with high μ_{H_2} and low μ_{H_2O}, so μ_O is low in this system and CoO surfaces can be reduced to Co^0 through the following reaction:

$$CoO + H_2 \rightarrow Co + H_2O \qquad (4)$$

At the other extreme, a system with high μ_{H_2O} and low μ_{H_2} is more oxidative and will facilitate the above reaction to proceed in the reverse direction. It should be noted that the argument above is also supported by recent experiments showing that H_2O can induce the oxidation of Co^0 into Co^{2+}.[16, 20, 25] Unlike previous studies which considered a H_2O/O_2 binary gas phase system[36, 44], in this study μ_O is not related to p_{O_2} since there is not an O_2 gas phase component in ESR reactions. Instead μ_O is determined by μ_{H_2O} and μ_H through the relation $\mu_{H_2O} = \mu_O + 2\mu_H$.

The chemical potentials of gas phase H_2 and H_2O were calculated by

$$\mu_{H_2(g)} = E^{DFT}_{H_2(g)} + E^{ZPC}_{H_2(g)} + \Delta G^0_{H_2(g)}(T) + RTln\frac{p_{H_2}}{p^0} \qquad (5)$$

$$\mu_{H_2O(g)} = E^{DFT}_{H_2O(g)} + E^{ZPC}_{H_2O(g)} + \Delta G^0_{H_2O(g)}(T) + RTln\frac{p_{H_2O}}{p^0} \qquad (6)$$

In the equations above, $E^{DFT}_{H_2(g)}$ is the DFT calculated electronic energy of an isolated H_2 molecule, and $E^{ZPC}_{H_2(g)}$ is its zero-point energy correction due to vibration. These two terms represent the Gibbs free energy of H_2 at 0 K. $\Delta G^0_{H_2(g)}(T)$ is defined as $\Delta G^0_{H_2(g)}(T) = G_{H_2(g)}(T, p^0) - G_{H_2(g)}(0\ K, p^0)$ and was obtained from thermodynamic tables[63]. The standard pressure, p^0, is chosen as 1 atm.

We assume that the slab structure is in equilibrium with bulk phase CoO, therefore the chemical potentials of Co and O must satisfy

$$\mu_{Co} + \mu_O = g^{bulk}_{CoO} \qquad (7)$$

Catalysis Science & Technology Accepted Manuscript

So eqn. (1) can be rewritten as

$$\gamma = \frac{1}{2A}[G^{slab} - N_{Co}g_{CoO}^{bulk} - (N_O - N_{Co})\mu_O - N_H\mu_H] \quad (8)$$

Free energy of the slab was calculated by standard thermodynamic methods [64-66]:

$$G^{slab} = E^{DFT} + E^{ZPC} + E^v - TS^v \quad (9)$$

In the above equation, the superscript DFT refers to its electronic energy directly calculated from DFT; ZPC refers to its zero-point energy correction; E_i^v and S_i^v refer to its vibrational contributions to the internal energy and the entropy. When calculating these terms, we did not consider the vibrational contributions from lattice Co and O atoms in the slabs. Correspondingly, we did not consider vibrational and entropic contributions to the free energy of bulk CoO. Since only the difference between G^{slab} and g_{CoO}^{bulk} enters into eqn. (8), vibrational and entropic contributions from lattice atoms in the slab and atoms in the bulk phase are assumed to be cancelled out, which is similar to the approach adopted by previous studies on Cu_2O [62], RuO_2[42], and PdO[67]. However we explicitly calculated the vibrational contributions from atoms adsorbated on the surfaces (in the case of CoO(111) all atoms above the first Co layer are considered to have vibrational contributions). Their vibrational frequencies were obtained from normal mode analysis after the structural relaxation using the VASP software.

Chemical potentials of H and O are directly related to the partial pressures of H_2O and H_2 through equations (2), (3), (5), and (6). Since we are interested in catalytic activity of CoO for ESR reactions, the allowed range of p_{H_2O} and p_{H_2} should be selected to cover ESR reaction conditions. The ESR reactions are usually operated under normal pressures using a mixture of steam and ethanol as the feed[6, 7]. Typical steam-to-ethanol ratio can be 10:1 or higher and the mixture is often diluted by an inert carrier gas such as Ar or He[7, 22].

Catalysis Science & Technology Accepted Manuscript

Based on these conditions p_{H_2O} should approximately range between 10^{-5} and 1 atm under ESR conditions. Similarly p_{H_2} should not exceed 1 atm. However p_{H_2} could be very small, for example 10^{-15} atm, at the entrance of plug flow type reactors. In this study we varied p_{H_2} between 10^{-20} and 10^{8} atm, and p_{H_2O} between 10^{-10} and 10^{8} to make sure the ESR reaction conditions were covered. In this paper we have also used $\Delta\mu_{H_2O}$ and $\Delta\mu_H$ to measure the chemical potentials of H_2O and H. They are defined as $\Delta\mu_{H_2O} = \mu_{H_2O} - E_{H_2O}$ and $\Delta\mu_H = \mu_H - \frac{1}{2}E_{H_2}$, where E_{H_2O} and E_{H_2} are the total energies of isolated H_2O and H_2 molecules at 0 K. In other words, they represent the latter two terms in eqn. (5) and (6). This definition is consistent with those used in previous studies [36, 44]. The allowed values of $\Delta\mu_{H_2O}$ and $\Delta\mu_H$, together with the stability of the CoO phase compared with the Co_3O_4 and metallic Co phases under these values, will be discussed in Section 3.1.

Catalysis Science & Technology Accepted Manuscript

3. Results and Discussion

3.1 Surface configurations of CoO(100)

The bulk phase of CoO has a rocksalt structure where both Co and O atoms are in octahedral sites. The (100) facet of CoO has only one type of termination, which is shown in Fig. 1(a). Under ESR reaction conditions, oxygen vacancies may form due to the reaction between the surface and gas phase H_2. Since we built a 2×2 periodic unit cell within which 4 surface oxygen atoms are present, we were able to model the CoO(100) surfaces with 0, 0.25, 0.5, 0.75, and 1 ML of oxygen vacancies. Figure 2(a) shows the structure of the clean CoO(100) surface without any oxygen vacancy. The structures of CoO(100) with 0.25 and 0.5 ML oxygen vacancies, referred to as 0.25 O-vac (100) and 0.5 O-vac (100), are shown in Fig. 2(b) and (c), respectively. Table 1 lists the reaction energies that are needed to create oxygen vacancies from the clean CoO(100) surface. As seen in Table 1, oxygen vacancy formation is highly endothermic on the CoO(100) facet, thus we did not consider structures with more than 0.5 ML oxygen vacancies.

In order to determine possible surface configurations of CoO under the presence of H_2O and H_2, we calculated the adsorption of H_2O and H_2 on CoO surfaces and considered the possible structures obtained from H_2O and H_2 dissociation. Reaction energies of relevant steps are also listed in Table 1. H_2O can adsorb on the clean CoO(100) surface by binding to a Co atom as shown in Fig. 2(d). The H_2O adsorption energy on the CoO(100) surface is -0.39 eV, which is quite similar to the -0.34 eV value found on the metallic Co(0001) surface [31]. However, H_2O* dissociation into OH* and H* (as shown in

Catalysis Science & Technology Accepted Manuscript

Fig. 2(e)) gives a reaction energy of 2.75 eV on the clean CoO(100) surface, which is very endothermic compared with the water dissociation energy of -0.62 eV found on Co(0001)[31]. To investigate the cause of this large energy difference, we further calculated the adsorption of OH* and H* on the clean CoO(100) surface (as shown in Fig. 2(f) and (g)). Both OH* and H* prefer to bind with a Co atom. The adsorption energies of OH* and H* are -2.08 eV and -1.12 eV referenced to the energies of isolated OH group and H atom. Compared with the adsorption energies of -3.65 and -2.81 eV for OH and H on the Co(0001) surface, adsorption of OH and H is strongly disfavored on the CoO(100) surface and results in the large endothermic dissociation energy of H_2O.

As will be discussed below, CoO(100) surface with O vacancies are found to be not stable under ESR conditions, therefore we did not further consider H_2O* adsorption and dissociation steps on O vacancy containing CoO(100) surfaces. We assume that the thermodynamically preferred reaction between H_2O and 0.25 O-vac CoO(100) is [0.25 O-vac CoO(100) + H_2O → clean CoO(100) + H_2] instead of H_2O* adsorption on 0.25 O-vac CoO(100).

With the possible surface configurations identified, we can generate a surface phase diagram, as shown in Fig. 3, to study the most stable configuration of the CoO(100) facet under ESR conditions. We used the typical ESR reaction temperature of 723 K when generating the diagram[12]. We also tested two other temperatures, namely 523 K and 923 K, but these cannot be shown in the same diagram with different p_{H_2}, p_{H_2O} (or $\Delta\mu_H, \Delta\mu_{H_2O}$) scales. Instead the results obtained at 523 and 923 K are given in the Supporting Information (Fig. S1 and S2). A discussion on how the temperature affects

Catalysis Science & Technology Accepted Manuscript

the surface stability is also given there (Section S2). We varied p_{H_2} and p_{H_2O} to cover possible conditions encountered in ESR reactions. However, the allowed ranges of $\Delta\mu_H$ and $\Delta\mu_{H_2O}$ are not without bound. The maximum allowed values of $\Delta\mu_{H_2O}$ is considered to be -0.91 eV, which represents to the critical point of H_2O[44]. At 723 K, this value corresponds to p_{H_2O} of 2.2×10^3 atm. $\Delta\mu_H$ should also be less than 0 eV (or $p_{H_2} < 4.7 \times 10^6$) to prevent the condensation of H on the surfaces. Furthermore, we also need to consider the stability of CoO in the bulk phase through the following two reactions:

$Co + H_2O \rightarrow CoO + H_2$ (10)

$3\ CoO + H_2O \rightarrow Co_3O_4 + H_2$ (11)

The bulk phase of CoO is stable compared with Co and Co_3O_4 only when

$$\Delta_r G(10) = g_{CoO}^{bulk} - g_{Co}^{bulk} + g_{H_2} - g_{H_2O} = \Delta_r G^0(10) - RTln\frac{p_{H_2O}}{p_{H_2}} < 0 \quad (12)$$

and

$$\Delta_r G(11) = g_{Co_3O_4}^{bulk} - 3g_{Co}^{bulk} + g_{H_2} - g_{H_2O} = \Delta_r G^0(11) - RTln\frac{p_{H_2O}}{p_{H_2}} > 0 \quad (13)$$

The reaction free energies of (10) and (11) under standard conditions can be obtained from thermodynamic tables[63], which shows that $\Delta_r G^o(10) = 0.259\ eV$ and $\Delta_r G^o(11) = 1.290\ eV$ at 723 K. Therefore if p_{H_2} and p_{H_2O} satisfy $63.5 < \frac{p_{H_2O}}{p_{H_2}} < 9.75 \times 10^8$, the CoO is stable compared with Co and Co_3O_4 in the bulk phase.

Two solid lines are shown in Fig. 3 to represent the maximal allowed potentials of H_2O ($\Delta\mu_{H_2O} < -0.91\ eV$) and H ($\Delta\mu_H < 0\ eV$) as discussed above. Within the region where the potentials of H_2O and H are allowed, the clean CoO(100) surface without oxygen vacancy occupies most of the area on this diagram. The H_2O* adsorption will only be possible when p_{H_2O}> 3.10×10^5 atm, or $\Delta\mu_{H_2O} > -0.61\ eV$, which exceeds the

Catalysis Science & Technology Accepted Manuscript

critical point of H_2O and is not possible under ESR reaction conditions. Only at very high potential of H_2O but very low potential of H, OH* adsorption can be formed. On the contrary, oxygen vacancy formation is only possible under very high H_2 and low H_2O potentials. Other surface configurations, such as H* adsorption, H* and OH* co-adsorption, and oxygen vacancies higher than 0.25 ML, are not stable in the range shown in Fig. 3. Under ESR reaction conditions, the only possible configuration on CoO(100) is the clean (100) surface.

Two dashed lines are drawn on Fig. 3 to mark the region where CoO is stable in the bulk phase. To the upper left of the "Bulk Co_3O_4 → Bulk CoO" line, Co_3O_4 is more stable in the bulk phase, while metallic Co is more stable in the bulk phase if the reaction condition is to the lower right of the "Bulk CoO → Bulk Co" line. It is interesting to note that the CoO(100) surface has quite different properties compared with bulk CoO. Although metallic Co becomes more stable than CoO in the bulk phase when $\frac{p_{H_2O}}{p_{H_2}} <$ 63.5, no oxygen vacancy can form on the CoO(100) surface until $\frac{p_{H_2O}}{p_{H_2}}$ becomes less than 2.87×10^{-12}. This result suggests that the CoO(100) surface has a different reducibility compared with bulk CoO. Similar observations were also reported in previous studies on RuO_2[43] and PdO[67]. For example Reuter et al. found that RuO_2(110)-Ru (partially reduced surface) is less stable than RuO_2(110)-O^{bridge} (Stoichiometric surface) even when $\Delta\mu_O$ is smaller than the limit where metallic Ru becomes favored in the bulk phase[43]. In section 3.3 we will revisit a general surface phase diagram that incorporates Co metal surfaces.

Catalysis Science & Technology Accepted Manuscript

3.2 Surface configurations of CoO(111)

CoO(111) has two possible terminations, namely the Co-terminated (Co-term) and O-terminated (O-term) CoO(111) surfaces. As suggested by previous studies, O-term CoO(111) may exhibit a special wurtzite type near surface structure, where the first layer of Co are in tetrahedral sites instead of octahedral sites [39, 68]. A comparison between O-term CoO(111) with rocksalt and wurtzite type near surface structures, after structural optimization using DFT, is shown in Fig. 4(a) and (b) in a style similar to Fig. 3 in Meyer et al.'s work[39]. We found that the wurtzite type O-term (111) is 18 meV/Å^2 more stable than the rocksalt type O-term (111). We also found that in wurtzite type O-term(111), the distances between the first two layers (d_{12}) and between the second and the third layer (d_{23}) are 0.67 and 1.82 Å, respectively, which are very close to experimentally determined values of 0.61 and 1.91 Å[39].

However, the wurtzite type near surface structure is stable only when the surface is fully covered by O. Even with 0.25 ML oxygen vacancies present, the wurtzite type structure (not shown in Fig. 4) becomes 13 meV/Å^2 less stable than its rocksalt counterpart (as shown in Fig. 4(c)). When the (111) facet is covered by 1 ML of OH* or 1 ML of H*, as will be discussed later, the near surface wurtzite structures are 75 and 38 meV/Å^2 less stable, respectively. Therefore in this study we considered the wurtzite structure only for perfectly O* covered CoO(111), but for all other surface configurations the rocksalt structure is used.

Similar to CoO(100), the 2×2 periodic unit cell we built for CoO(111) allowed us to study the surfaces with 0.25, 0.5, and 0.75 ML of oxygen vacancies. We show these structures in Fig. 4(c), (d), and (e) and refer to them as 0.75 O* (111), 0.5 O* (111), and

Catalysis Science & Technology Accepted Manuscript

0.25 O* (111), respectively, since their structures are equivalent to the Co terminated CoO(111) surfaces covered by 0.75, 0.5, and 0.25 ML of oxygen atoms. Table 2 lists the reaction energies that are necessary to create these oxygen vacancies as predicted by our DFT calculations. Contrary to CoO(100), creation of oxygen vacancies of 0.25 and 0.5 ML is exothermic, but beyond 0.5 ML the formation of oxygen vacancies becomes endothermic.

The behavior of H_2O and H_2 adsorption and dissociation is very different on CoO(111) versus CoO(100). Since we built a 2×2 unit cell for CoO(111), the Co-term CoO(111) (as shown in Fig. 4(f)) can be viewed as a surface with four possible adsorption sites in each unit cell. Any other CoO(111) surface configuration can be obtained by filling one or several adsorption sites on the Co-term surface with O*, OH* or H*. These configurations include but are not limited to those shown in Fig. 4, such as a surface fully covered by OH* (Fig. 4(h)), a surface covered by a mixture of OH* and H* (Fig. 3(l)), or a surface covered by a mixture of OH*, H* and O* (Fig. 3(i)). Table 2 lists some of the reaction energies that are needed to convert these structures to each other.

From Table 2 it can be seen that both the O-term CoO(111) and the Co-term CoO(111) can react with H_2 and H_2O to generate OH* and H* adsorption. If only judged by the reaction energies, the most stable configuration should be a surface fully covered by OH*. The transition from 1.0 OH* to 0.75 OH*, 0.25 H* is slightly endothermic by 0.39 eV, but substitution of O* with OH* and H* is always exothermic.

The surface phase diagram of CoO(111) incorporating all these possible surface terminations is shown in Fig. 5. Similar to Fig. 3, two dashed lines mark the boundaries

Catalysis Science & Technology Accepted Manuscript

where CoO is the most stable bulk phase compared with Co and Co_3O_4. The upper right portion of this diagram, which represents the condition under which both H_2O and H_2 are abundant, is occupied by the OH* covered CoO(111) surface configuration. If p_{H_2} is kept at high values (> 10^{-2} atm) but p_{H_2O} is lowered, a gradual transition from OH* adsorption to H* adsorption, together with some mixed OH*, H* adsorption with different OH*/H* ratios, can be observed on the CoO(111) facet. On the left side of this diagram, fully O* covered surface configuration is stable at low p_{H_2} and p_{H_2O} conditions. As the reaction condition turns more reductive, lower O* coverages such as 0.5 O* and 0.25 O* can be observed on the diagram.

Catalysis Science & Technology Accepted Manuscript

3.3 General surface phase diagram for the Co^0/Co^{2+} catalyst

In the previous sections, we have presented the surface phase diagrams of CoO(100) and CoO(111), however we did not compare the stability of these two facets against each other. More importantly, under ESR reaction conditions it is assumed that both the metallic Co and CoO phases can exist, therefore it is necessary to account for the phase changes and compare surface configurations based on the CoO bulk structure with those based on the metallic Co bulk structure.

We chose the (0001) facet to represent the metallic Co surface. In addition to the clean Co(0001) surface, we also considered the Co(0001) surfaces adsorbed by 0.25 ML of OH* or H*, as well as a surface covered by the co-adsorption of OH*, H*. The calculated adsorption energies of OH* (-3.63 eV) and H* (-2.65 eV) are quite similar to previously found values of -3.65 and -2.81 eV by Ma et al.[31]

In Fig. 6 we give a general surface phase diagram for the Co^0/Co^{2+} catalytic system. The method we used to constructed this diagram is similar to the one proposed by Su et al.[69] and is described in detail in the Supporting Information (Section S1).

Similar to Fig. 3 and 5, two dashed lines mark the boundaries where transitions from Co_3O_4 to CoO and from CoO to Co are thermodynamically favored in the bulk phase. Since we are only interested in the Co^0/Co^{2+} catalytic system, no surface configuration based on Co_3O_4 was included in this diagram, but the readers should keep in mind that Co_3O_4 phase based surfaces should form if the reaction condition goes beyond the Co_3O_4 → CoO phase transition line marked in Fig. 6. In the region where CoO is stable in the bulk phase, the clean CoO(100) surface is thermodynamically more favorable until p_{H_2O} reaches 47.1 atm, above which the fully OH* covered CoO(111) surface becomes more

Catalysis Science & Technology Accepted Manuscript

stable. Therefore, under normal ESR operation conditions where both p_{H_2O} and p_{H_2} are less than 1 atm, CoO(100) facet is always more stable than the CoO(111) facet. As the reaction condition becomes more reductive, a transition from CoO surface configurations to Co surface configurations can be observed. On this surface phase diagram it is evident that the transition of CoO surfaces to metallic Co surfaces almost strictly follows the CoO → Co bulk phase transition line. Under normal ESR operation conditions (p_{H_2O}, $p_{H_2} < 1\ atm$), the clean Co(0001) is the most stable configuration of metallic Co surface. As p_{H_2} increases, H* adsorption can develop on the surface, while OH* adsorption or OH*, H* co-adsorption can be found as p_{H_2O} increases.

Although the surface phase diagram is useful in determining the most stable surface configurations under different conditions, it does not provide quantitative information about by what degree one configuration is more stable than other ones. An interesting case is the relative stability between CoO(100) and CoO(111). In fact, the surface free energies of clean CoO(100) and 1.0 OH* CoO(111) are quite close to each other. For example, at $p_{H_2O} = 1$ and $p_{H_2} = 0.01$ atm we have $\gamma_{clean\ CoO(100)}$ = 0.046 eV/Å^2, while $\gamma_{1.0\ OH^*CoO(111)}$ = 0.062 eV/Å^2 at the same condition, which is only slightly less stable than the CoO(100) facet. The fact that the (100) facet is more stable does not mean the absence of the (111) facet on the catalyst surfaces, instead these two facets can reach a thermodynamic equilibrium under ESR reaction conditions, and the relative ratio between their exposed areas can be estimated by methods such as the Wulff construction. Since CoO(100) and CoO(111) can show different catalytic activities towards ESR reactions, for example in the Supporting Information (Section S4) we compared ethanol dehydrogenation on these two facets, increasing the area of the more active facet may

Catalysis Science & Technology Accepted Manuscript

improve the performance of Co catalysts. Such tailoring of the facet area can possibly be achieved by using a support material with special morphologies that preferentially favors one facet over the other. For example, Giovanardi et al. showed that the Ir(100) surface selectively favors the growth of CoO in the (111) orientation[70].

Catalysis Science & Technology Accepted Manuscript

4. Conclusions

In this study we examined the stability of various surface configurations based on CoO(100), CoO(111) and Co(0001). Under ESR reaction conditions, the most stable surface configurations for CoO(100) and CoO(111) are the clean CoO(100) surface and the OH* covered CoO(111) surface, respectively. OH* and H* mixed covered CoO(111) may also be stable if p_{H_2} is high or hydrogen production reactions, such as ESR, occur on the surface. Further DFT studies of the elementary steps of ESR on CoO should mainly focus on these structures. We also noticed that the (111) facet is slightly less stable than the (100) facet of CoO, which suggests that the (111) facet will have a smaller surface area compared with CoO(100) if thermodynamic equilibrium between these two facets are reached. If future studies show that one of these two facets has higher ESR catalytic activity, measures can be taken to stabilize the more active facet, for example in the manner suggested by Giovanardi et al.[70], to increase the performance of the Co-based catalysts.

We also observed that the transition condition from CoO to Co is approximately at $\frac{p_{H_2O}}{p_{H_2}} = 10^2$ both on the surface and in the bulk phase, and this condition does not change as temperature varies (as explained in Section S2). However under ESR reaction conditions, unless at the entrance point of a plug flow type reactor, it is very easy for p_{H_2} to be higher than 0.01 times p_{H_2O}. If the hydrogen conversion rate is high, it is even common for p_{H_2} to be greater than p_{H_2O}. Under these conditions, there may be a deficit of the Co^{2+} phase and potentially this may be the reason for the low activities reported for unsupported Co or non-reducible material supported Co such as Co/ZrO_2[17]. The presence

Catalysis Science & Technology Accepted Manuscript

of a reducible support such as CeO_2 or ZnO may help to stabilize the CoO surfaces and promote ESR catalytic activities, but to test such a hypothesis will require mapping out the stability of CoO phases on oxide supports, as well as the role of CoO surfaces in the activity of ESR.

All results in this paper are based on thermodynamics but kinetics may play an important role in determining the surface structures. Furthermore, surface oxides of cobalt may be stable thermodynamically or kinetically versus the metal and bulk oxide phases. Future experimental and theoretical studies will be needed to determine if surface oxides are present under reaction conditions. Nevertheless, this study provides a basis for further DFT investigations of the catalytic activity of Co^{2+} in ESR reactions. Hypothesis about the specific roles of Co^{2+}, such as the facilitation of ethoxide dehydrogenation into acetaldehyde[28], can be tested on the CoO structures that are found to be most stable under ESR conditions in this study. The role of the support on the relative stability of Co^{2+}/Co^0 also needs to be explored in future studies.

Acknowledgement

We are grateful for the computational resources provided by the Ohio Supercomputer Center (OSC).

Catalysis Science & Technology Accepted Manuscript

References

1 S. J. McPhail, V. Cigolotti, A. Moreno and L. Jörissen, Springer London, Editon edn., 2012, pp. 189-203.
2 M. Ni, D. Y. C. Leung and M. K. H. Leung, *Int. J. Hydrogen Energy*, 2007, **32**, 3238-3247.
3 H. Song and U. S. Ozkan, *Int. J. Hydrogen Energy*, 2010, **35**, 127-134.
4 D. K. Liguras, D. I. Kondarides and X. E. Verykios, *Appl. Catal., B*, 2003, **43**, 345-354.
5 J. E. Sutton, P. Panagiotopoulou, X. E. Verykios and D. G. Vlachos, *J. Phys. Chem. C*, 2013, **117**, 4691-4706.
6 F. Haga, T. Nakajima, H. Miya and S. Mishima, *Catal. Lett.*, 1997, **48**, 223-227.
7 J. Llorca, N. Homs, J. Sales and P. R. de la Piscina, *J. Catal.*, 2002, **209**, 306-317.
8 J. Llorca, P. R. de la Piscina, J.-A. Dalmon, J. Sales and N. Homs, *Appl. Catal., B*, 2003, **43**, 355-369.
9 M. S. Batista, R. K. S. Santos, E. M. Assaf, J. M. Assaf and E. A. Ticianelli, *J. Power Sources*, 2004, **134**, 27-32.
10 H. Song, L. Zhang, R. B. Watson, D. Braden and U. S. Ozkan, *Catal. Today*, 2007, **129**, 346-354.
11 S. Lin, D. Kim and S. Ha, *Catal. Lett.*, 2008, **122**, 295-301.
12 H. Song, B. Tan and U. S. Ozkan, *Catal. Lett.*, 2009, **132**, 422-429.
13 H. Song and U. S. Ozkan, *J. Mol. Catal. A: Chem.*, 2010, **318**, 21-29.
14 H. Song, B. Mirkelamoglu and U. S. Ozkan, *Appl. Catal., A*, 2010, **382**, 58-64.
15 J. Llorca, N. Homs and P. Ramirez de la Piscina, *J. Catal.*, 2004, **227**, 556-560.
16 H. Song and U. S. Ozkan, *J. Phys. Chem. A*, 2010, **114**, 3796-3801.
17 H. Song and U. S. Ozkan, *J. Catal.*, 2009, **261**, 66-74.
18 J. Llorca, J.-A. Dalmon, P. Ramírez de la Piscina and N. s. Homs, *Appl. Catal., A*, 2003, **243**, 261-269.
19 S. Tuti and F. Pepe, *Catal. Lett.*, 2008, **122**, 196-203.
20 S. S. Y. Lin, D. H. Kim, M. H. Engelhard and S. Y. Ha, *J. Catal.*, 2010, **273**, 229-235.
21 S. S. Y. Lin, D. H. Kim and S. Y. Ha, *Appl. Catal., A*, 2009, **355**, 69-77.
22 B. Bayram, I. I. Soykal, D. von Deak, J. T. Miller and U. S. Ozkan, *J. Catal.*, 2011, **284**, 77-89.
23 V. A. de la Peña O'Shea, N. Homs, E. B. Pereira, R. Nafria and P. Ramírez de la Piscina, *Catal. Today*, 2007, **126**, 148-152.
24 M. S. Batista, R. K. S. Santos, E. M. Assaf, J. M. Assaf and E. A. Ticianelli, *J. Power Sources*, 2003, **124**, 99-103.
25 A. M. Karim, Y. Su, M. H. Engelhard, D. L. King and Y. Wang, *ACS Catal.*, 2011, **1**, 279-286.
26 A. R. Passos, L. Martins, S. H. Pulcinelli, C. V. Santilli and V. Briois, *Catal. Today*.
27 C. N. Avila-Neto, J. W. C. Liberatori, A. M. da Silva, D. Zanchet, C. E. Hori, F. B. Noronha and J. M. C. Bueno, *J. Catal.*, 2012, **287**, 124-137.
28 E. Martono and J. M. Vohs, *ACS Catal.*, 2011, **1**, 1414-1420.
29 E. Martono and J. M. Vohs, *J. Catal.*, 2012, **291**, 79-86.
30 E. Martono, M. P. Hyman and J. M. Vohs, *Phys. Chem. Chem. Phys.*, 2011, **13**, 9880-9886.
31 Y. Ma, L. Hernández, C. Guadarrama-Pérez and P. B. Balbuena, *J. Phys. Chem. A*, 2012, **116**, 1409-1416.
32 J.-H. Wang, C. S. Lee and M. C. Lin, *J. Phys. Chem. C*, 2009, **113**, 6681-6688.
33 D.-e. Jiang and S. Dai, *Phys. Chem. Chem. Phys.*, 2011, **13**, 978-984.

Catalysis Science & Technology Accepted Manuscript

34 H.-F. Wang, R. Kavanagh, Y.-L. Guo, Y. Guo, G.-Z. Lu and P. Hu, *Angew. Chem. Int. Ed.*, 2012, **51**, 6657-6661.
35 M. García-Mota, M. Bajdich, V. Viswanathan, A. Vojvodic, A. T. Bell and J. K. Nørskov, *J. Phys. Chem. C*, 2012, **116**, 21077-21082.
36 M. Fronzi, S. Piccinin, B. Delley, E. Traversa and C. Stampfl, *Phys. Chem. Chem. Phys.*, 2009, **11**, 9188-9199.
37 C. Mocuta, A. Barbier and G. Renaud, *Appl. Surf. Sci.*, 2000, **162–163**, 56-61.
38 S. C. Petitto, E. M. Marsh, G. A. Carson and M. A. Langell, *J. Mol. Catal. A: Chem.*, 2008, **281**, 49-58.
39 W. Meyer, D. Hock, K. Biedermann, M. Gubo, S. Müller, L. Hammer and K. Heinz, *Phys. Rev. Lett.*, 2008, **101**, 016103.
40 V. I. Anisimov, J. Zaanen and O. K. Andersen, *Phys. Rev. B*, 1991, **44**, 943-954.
41 I. A. Vladimir, F. Aryasetiawan and A. I. Lichtenstein, *J. Phys.: Condens. Matter*, 1997, **9**, 767.
42 K. Reuter and M. Scheffler, *Phys. Rev. B*, 2003, **68**, 045407.
43 K. Reuter and M. Scheffler, *Phys. Rev. B*, 2001, **65**, 035406.
44 Q. Sun, K. Reuter and M. Scheffler, *Phys. Rev. B*, 2003, **67**, 205424.
45 W. Jauch, M. Reehuis, H. J. Bleif, F. Kubanek and P. Pattison, *Phys. Rev. B*, 2001, **64**, 052102.
46 H. J. Monkhorst and J. D. Pack, *Phys. Rev. B*, 1976, **13**, 5188-5192.
47 V. A. de la Pena O'Shea, I. de P.R. Moreira, A. Roldán and F. Illas, *J. Chem. Phys.*, 2010, **133**, 024701.
48 W. L. Roth, *Phys. Rev.*, 1958, **110**, 1333-1341.
49 H.-X. Deng, J. Li, S.-S. Li, J.-B. Xia, A. Walsh and W. Su-Huai, *Appl. Phys. Lett.*, 2010, **96**, 162508-162508-162503.
50 A. Bshish, Z. Yaakob, B. Narayanan, R. Ramakrishnan and A. Ebshish, *Chem. Pap.*, 2011, **65**, 251-266.
51 U. D. Wdowik and K. Parlinski, *Phys. Rev. B*, 2007, **75**, 104306.
52 L. Wang, T. Maxisch and G. Ceder, *Phys. Rev. B*, 2006, **73**, 195107.
53 S. Dudarev, G. Botton, S. Savrasov, C. Humphreys and A. Sutton, *Phys. Rev. B*, 1998, **57**, 1505-1509.
54 Z. Hu and H. Metiu, *J. Phys. Chem. C*, 2011, **115**, 5841-5845.
55 S. Lutfalla, V. Shapovalov and A. T. Bell, *J. Chem. Theory Comput.*, 2011, **7**, 2218-2223.
56 G. Kresse and J. Furthmüller, *Comput. Mater. Sci.*, 1996, **6**, 15-50.
57 G. Kresse and J. Hafner, *Phys. Rev. B: Condens. Matter Mater. Phys.*, 1993, **47**, 558.
58 G. Kresse and D. Joubert, *Phys. Rev. B*, 1999, **59**, 1758.
59 P. E. Blöchl, *Phys. Rev. B*, 1994, **50**, 17953.
60 J. P. Perdew, K. Burke and M. Ernzerhof, *Phys. Rev. Lett.*, 1996, **77**, 3865-3868.
61 D. Sheppard, R. Terrell and G. Henkelman, *J. Chem. Phys.*, 2008, **128**, 134106.
62 A. Soon, M. Todorova, B. Delley and C. Stampfl, *Phys. Rev. B*, 2007, **75**, 125420.
63 M. W. Chase, *NIST-JANAF thermochemical tables*, 4 edn., American Institute of Physics, 1998.
64 G. Jones, J. G. Jakobsen, S. S. Shim, J. Kleis, M. P. Andersson, J. Rossmeisl, F. Abild-Pedersen, T. Bligaard, S. Helveg and B. Hinnemann, *J. Catal.*, 2008, **259**, 147-160.
65 C. J. Cramer, *Essentials of computational chemistry: theories and models*, John Wiley & Sons Inc, 2004.
66 D. A. McQuarrie and J. D. Simon, *Molecular thermodynamics*, Univ Science Books, 1999.

Catalysis Science & Technology Accepted Manuscript

67 J. Rogal, K. Reuter and M. Scheffler, *Phys. Rev. B*, 2004, **69**, 075421.
68 R. Hanafin, T. Archer and S. Sanvito, *Phys. Rev. B*, 2010, **81**, 054441.
69 H.-Y. Su, Y. Gorlin, I. C. Man, F. Calle-Vallejo, J. K. Norskov, T. F. Jaramillo and J. Rossmeisl, *Phys. Chem. Chem. Phys.*, 2012, **14**, 14010-14022.
70 C. Giovanardi, L. Hammer and K. Heinz, *Phys. Rev. B*, 2006, **74**, 125429.

Catalysis Science & Technology Accepted Manuscript

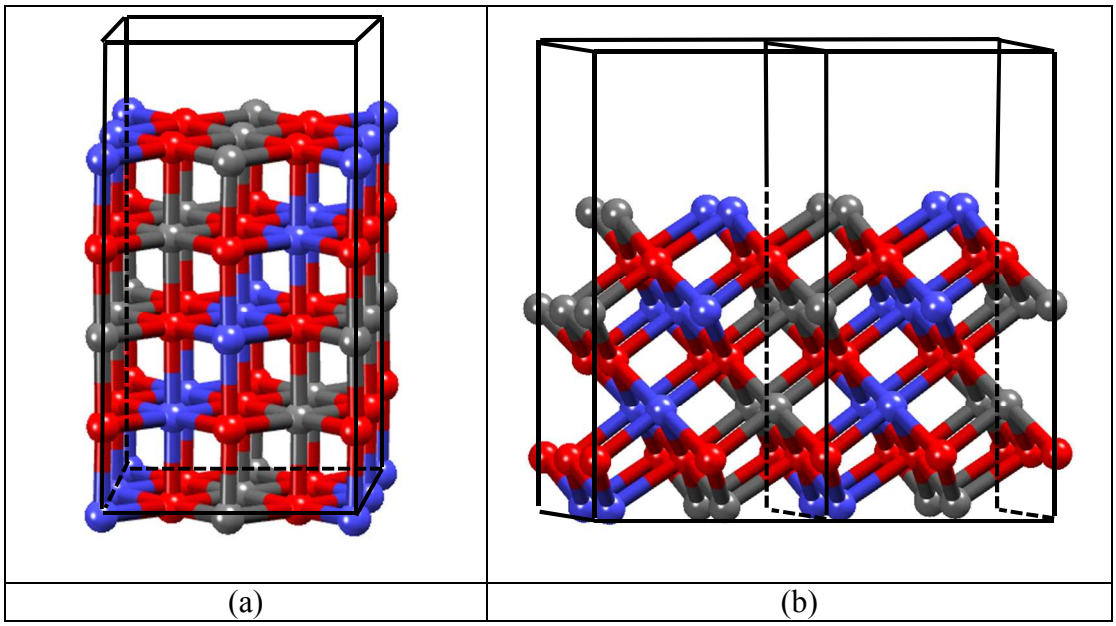

Fig. 1. Supercell structures of (a) CoO(100) and (b) Co-term CoO(111) used in this study. Red, blue, and grey balls represent O atoms, Co atoms with up spins, and Co atoms with down spins. Black lines are the boundaries of periodic unit cells. For CoO(111) two adjacent unit cells are shown to demonstrate its periodicity.

Catalysis Science & Technology Accepted Manuscript

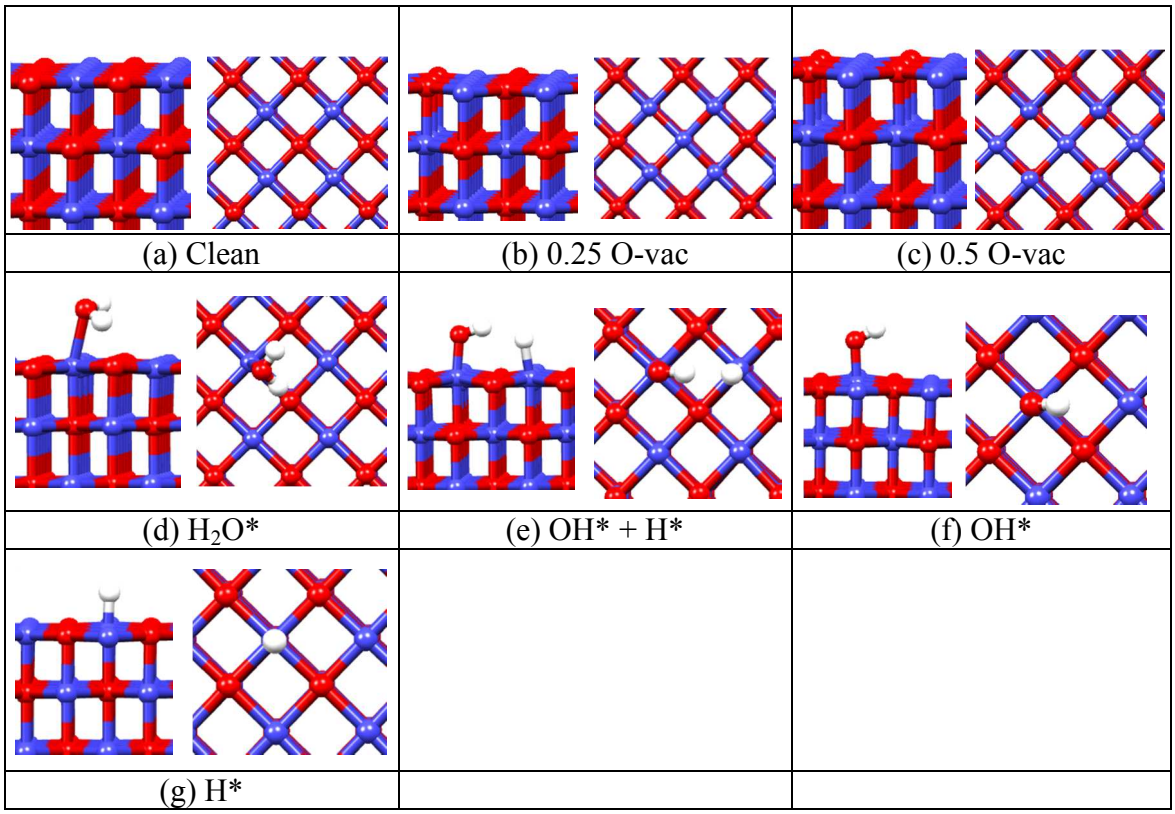

Fig. 2. Side and top views of optimized structures of CoO(100) facet with different configurations. Red, blue, and white balls represent O, Co, and H atoms.

Catalysis Science & Technology Accepted Manuscript

Table 1. DFT calculated reaction energies of transition between different CoO(100) surface configurations. Pictures for relevant structures are shown in Fig. 1.

Reaction	ΔE (eV)
clean + H_2 → 0.25 O-vac + H_2O	1.79
0.25 O-vac + H_2 → 0.5 O-vac + H_2O	1.54
clean + H_2O → H_2O*	-0.39
H_2O* → OH* + H*	2.75
clean + H_2 → 2H*	2.44
H_2O* → OH* + ½ H_2	1.56
clean + ½ H_2 → H*	1.20

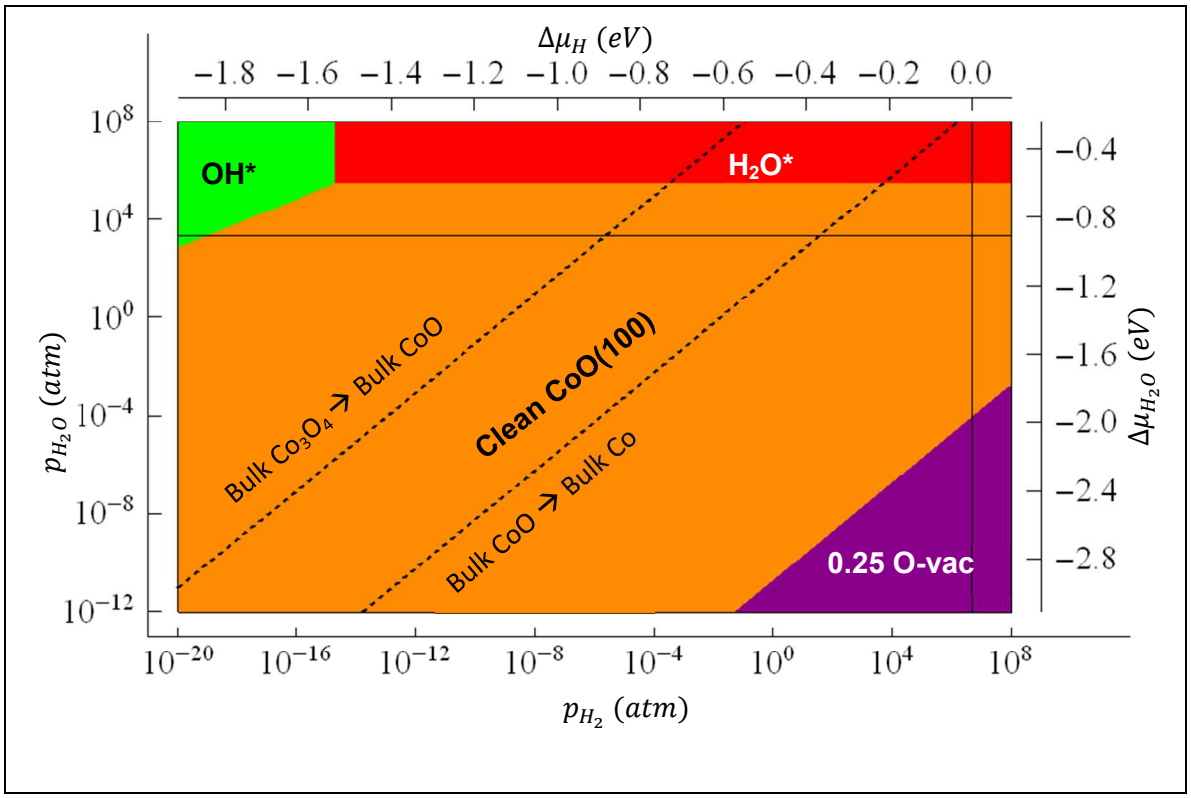

Fig. 3. Surface phase diagram of CoO(100) at 723 K. The black dashed lines mark the region where CoO is more stable than Co and Co_3O_4 in the bulk phase. The black solid lines represent the maximal allowed values of $p_{H_2O}(\Delta\mu_{H_2O})$ and $p_{H_2}(\Delta\mu_{H_2})$. These lines also appear in Fig. 5 and 6 and their meanings are the same.

Catalysis Science & Technology Accepted Manuscript

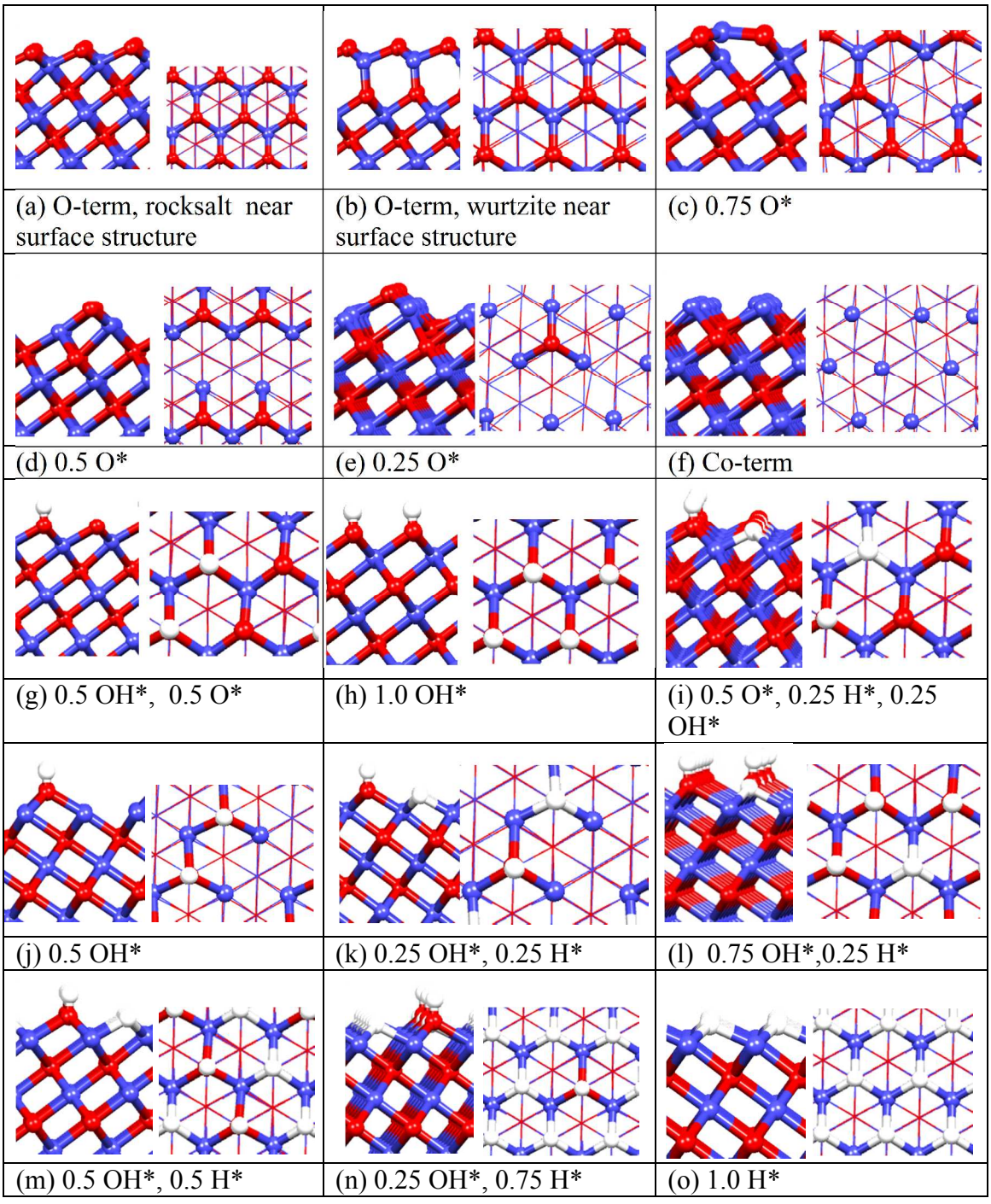

Fig. 4. Side and top views of optimized structures of CoO(111) facet with different configurations. Red, blue, and white balls represent O, Co, and H atoms. For clarity, atoms below the first Co layers are shown in line models in the top views.

Catalysis Science & Technology Accepted Manuscript

Table 2. DFT calculated reaction energies of transition between different CoO(111) surface configurations. Pictures for relevant structures are shown in Fig. 2.

Reaction	ΔE (eV)
O-term + H_2 → 0.75 O* + H_2O	-0.39
0.75 O* + H_2 → 0.5 O* + H_2O	-1.05
0.5 O* + H_2 → 0.25 O* + H_2O	0.85
0.25 O* + H_2 → Co-term + H_2O	1.22
0.5 OH*, 0.5 O* + H_2 → 4 OH*	-2.59
0.5 O* + H_2O → 0.25 OH*, 0.25 H*, 0.5 O*	-0.49
Co-term + H_2O → 0.25 OH*, 0.25 H*	-2.31
Co-term + H_2 → 0.5 H*	-1.36
1.0 OH* + H_2 → 0.75 OH*,0.25 H* + H_2O	0.39
0.75 OH*, 0.25 H* + H_2 → 0.5 OH*, 0.5 H* + H_2O	0.62
0.5 OH*, 0.5 H* + H_2 → 0.25 OH*, 0.75 H* + H_2O	0.71
0.25 OH*, 0.75 H* + H_2 → 1.0 H* + H_2O	0.88

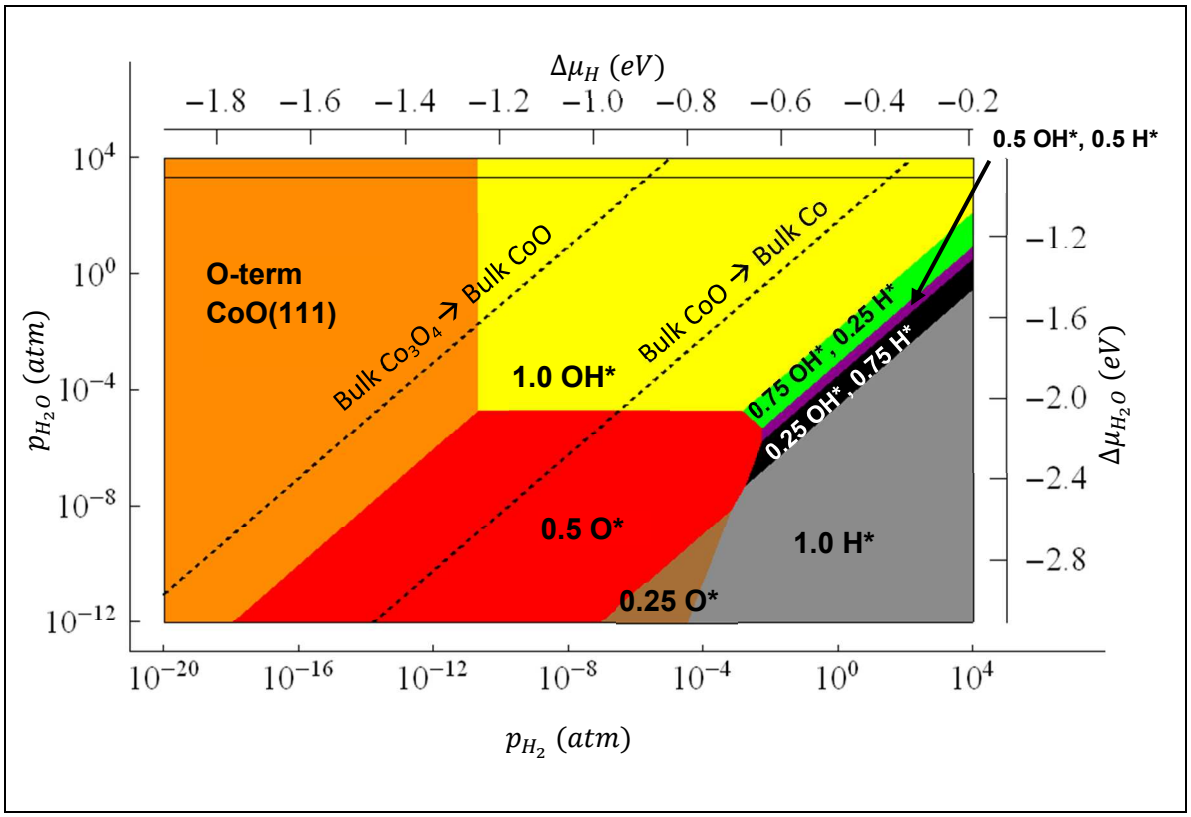

Fig. 5. Surface phase diagram of CoO(111) at 723K.

Catalysis Science & Technology Accepted Manuscript

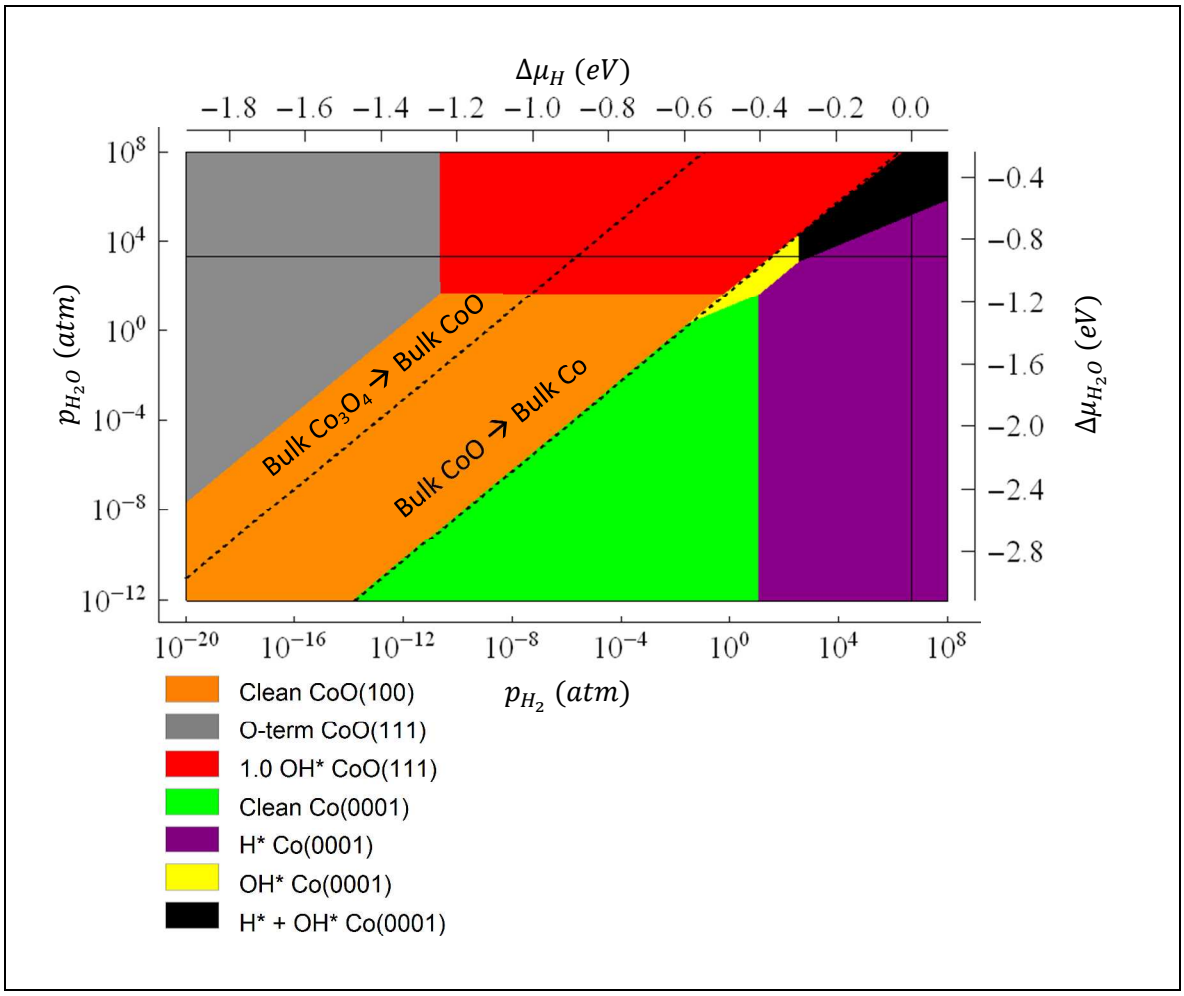

Fig. 6. General surface phase diagram of the Co^0/Co^{2+} catalyst at 723 K.

Catalysis Science & Technology Accepted Manuscript

TOC image

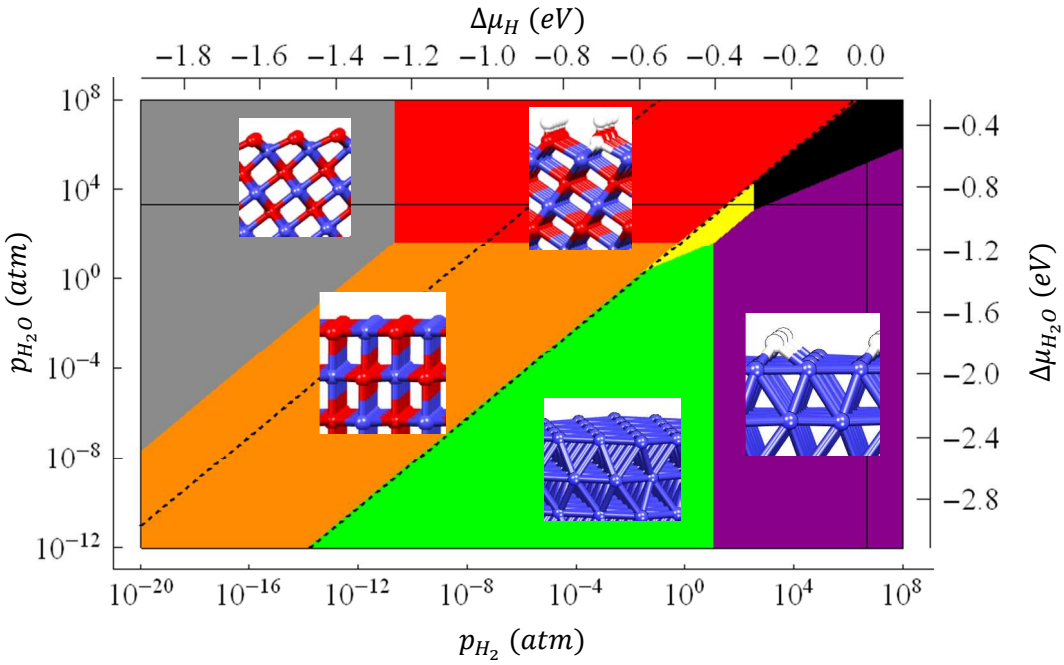

A combination of DFT and *ab intio* atomistic thermodynamics study illustrated the surface structure evolution of Co^0/Co^{2+} catalysts under ethanol steam reforming conditions.

Catalysis Science & Technology Accepted Manuscript

TOC image

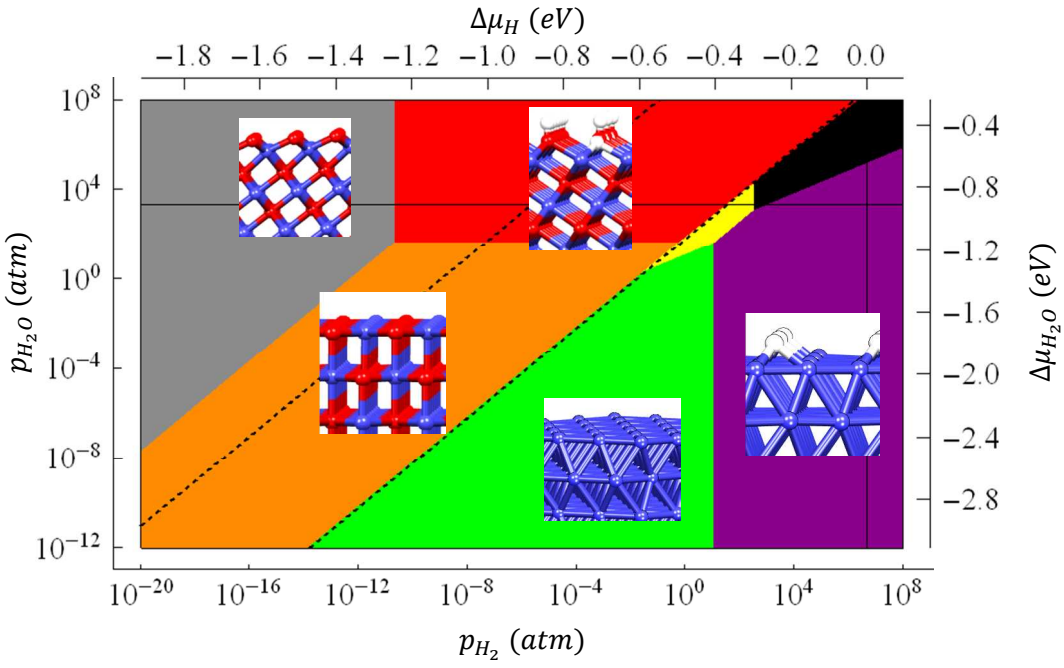

A combination of DFT and *ab intio* atomistic thermodynamics study illustrated the surface structure evolution of Co^0/Co^{2+} catalysts under ethanol steam reforming conditions.

Catalysis Science & Technology Accepted Manuscript